

Nucleic Acid Aptamers for Human Norovirus GII.4 and GII.17 Virus-Like Particles (VLPs) Exhibit Specific Binding and Inhibit VLPs from Entering Cells

Chao Cheng^{1,*}, Minjia Sun^{1-3,*}, Jingjing Li^{1,*}, Yitong Xue¹, Xia Cai⁴, Jing Liu¹, Xiaolian Wang⁵, Shouhong Xu², Youhua Xie¹, Junqi Zhang¹

¹MOE/NHC/CAMS Key Laboratory of Medical Molecular Virology, Shanghai Institute of Infectious Disease and Biosecurity, School of Basic Medical Sciences, Fudan University, Shanghai, 200032, People's Republic of China; ²Key Laboratory for Advanced Materials and Department of Chemistry, East China University of Science and Technology, Shanghai, 200237, People's Republic of China; ³Zhejiang CONBA Pharmaceutical Co., Ltd, Hangzhou, 310052, People's Republic of China; ⁴Shanghai Medical College, Biosafety Level 3 Laboratory, Fudan University, Shanghai, 200032, People's Republic of China; ⁵Department of Pathogen Microbiology and Preventive Medicine, School of Medicine, Hexi University, Zhangye, 734000, People's Republic of China

*These authors contributed equally to this work

Correspondence: Junqi Zhang, Email junqizhang@fudan.edu.cn; Youhua Xie, Email yhxie@fudan.edu.cn

Purpose: Human noroviruses (HuNoVs) are the main cause of non-bacterial acute gastroenteritis. Due to antigenic diversity, the discovery of ligands that can sensitively and specifically detect HuNoVs remains challenging. Limited by laboratory culture, no vaccines or drugs have been developed against HuNoVs. Here, we screened nucleic acid aptamers against the widespread HuNoV GII.4 and emerging HuNoV GII.17.

Methods: After ten rounds of sieving for HuNoV GII.4 and GII.17 virus-like particles (VLPs), eight ssDNA aptamers were generated and characterized for each genotype.

Results: Four of the eight aptamers generated for GII.4 VLP had dissociation constants (K_d) less than 100 nM, and all aptamers for GII.17 VLP had K_d less than 10 nM. All aptamers bound to their targets in VLP concentration-dependent manner. Two aptamers (AP4-2 and AP17-4) were selected for enzyme-linked aptamer sorbent assay (ELASA) and further analysis. Binding affinity was enhanced as the concentration of both aptamer and VLPs increased. The specificity of the aptamers was verified by ELASA and dot blotting. AP4-2 and AP17-4 were able to differentiate HuNoV from other diarrhea-causing pathogens or unrelated proteins ($P < 0.0001$). VLP/porcine gastric mucin (PGM) binding blockade assays revealed that AP4-2 and AP17-4 blocked the binding of HuNoV VLPs to PGM. VLP internalization inhibition assays showed that at a concentration of 0.5 μ M, both AP4-2 and AP17-4 effectively inhibited attachment and internalization of HuNoV VLPs into 293T cell ($P < 0.05$). Cell viability assays confirmed that aptamers did not induce cellular toxicity.

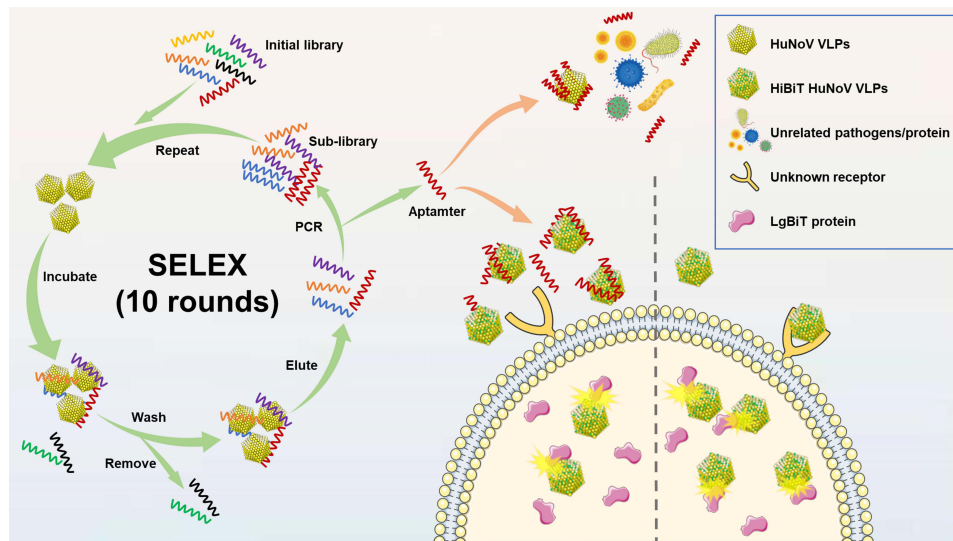
Conclusion: AP4-2 and AP17-4 showed strong affinity and specificity for their target VLPs and represent promising candidates for HuNoV capture and detection. This is the first study to demonstrate that aptamers can effectively inhibit HuNoV VLPs from binding to or entering cells, thus providing a new concept for the treatment of HuNoVs.

Keywords: human norovirus, SELEX, aptamer, diagnostics, therapeutics

Introduction

Human noroviruses (HuNoVs) belong to the *Caliciviridae* family and the *Norovirus* genus. These viral particles exhibit an icosahedral symmetric structure ($T = 3$), are 25–40 nm in diameter,^{1,2} and possess a viral genome containing approximately 7.5–8.3 kb positive-sense single-stranded RNA. HuNoVs are the main pathogen that causes non-bacterial acute enteritis in humans, with approximately 685 million diarrheal episodes occurring each year globally,

Graphical Abstract



resulting in 900,000 hospitalizations and more than 200,000 deaths.³ HuNoVs are highly contagious and environmentally stable,^{4–7} and can be transmitted by human-to-human, foodborne, waterborne and environmental routes.⁸ Most cases are caused by the GII.4 genotype in the GII gene group,⁹ which is associated with more than 50% of outbreaks globally.¹⁰ Beginning in the winter of 2014/2015, experienced the emergence of the GII.17 strain (GII.17 Kawasaki) that was able to escape population immunity in Asia, thus resulting in widespread outbreaks in China and Japan and even replacing GII.4 in some areas.^{11,12} In immunocompetent subjects, norovirus usually causes acute and self-limiting infections. However, immunocompromised subjects or the recipients of solid organ transplants (SOTs) can develop more severe and sometimes chronic noroviral infections, with viral shedding that can last for weeks to years.^{13,14} However, due to the diversity of HuNoV antigens and the difficulty of culturing these particles under laboratory conditions, there are currently no vaccines or drugs against HuNoVs.¹⁵

Despite the fact that HuNoVs were discovered over 50 years ago, none of the cell lines developed for this virus have been cultured successfully in the laboratory.^{16,17} Although stem cells or tissue-derived human intestinal organoids or human intestinal enteroids have been shown to be effective in culturing HuNoVs,¹⁸ these practices are limited to some specific genotypes^{19,20} and are expensive and demanding. Consequently, these methods have yet to be commonly utilized for vaccine development and drug screening. HuNoVs virus-like particles (VLPs) are morphologically and antigenically similar to real HuNoVs isolated from feces^{21–25} and can be generated by various expression systems, including baculovirus,²⁶ *Escherichia coli*,²⁷ and vesicular stomatitis virus (VSV),²⁸ which now play an important role in the development of vaccines for HuNoVs.

Since the infectious dose of HuNoVs is <100 copies,^{29,30} accurate and sensitive detection is vital if we are to prevent outbreaks. There are three main detection methods for HuNoVs: (1) observation by transmission electron microscopy, (2) real-time reverse transcription polymerase-chain reaction (RT-qPCR)-based amplification of gene fragments at the ORF1/ORF2 junction of the HuNoVs genome,^{31–34} and (3) antibody-based enzyme-linked immunosorbent assay (ELISA).³⁵ Of these, transmission electron microscopy provides clear observation of the morphology of typical HuNoVs particles, but is limited by high equipment requirements and running costs. RT-qPCR is highly sensitive but viral pre-processing, such as RNA extraction, takes a long time, and may produce false negatives for low concentrations of HuNoV in samples. Furthermore, because detection is only aimed at specific fragments of genes rather than full-field sequences, some gene fragments with no capsid wrapping may also be defined as pathogenic, thereby overestimating the infectivity of a given sample.³⁶ ELISA provides good portability; however, due to the broad antigenicity of HuNoVs, this method is

disadvantaged by low levels of sensitivity.^{35,37,38} Some candidate ligands for HuNoVs, such as histological blood group antigens (HBGAs) and porcine gastric mucosal proteins (PGMs) react with some, but not all, types of HuNoVs. In the current study, the inactivation of Norwalk virus GI.1 in oysters by high-pressure treatment, as estimated by PGMs combined with RT-qPCR, compared favorably with the results of parallel human challenge studies.^{39,40} However, PGMs are not applicable for practical testing due to their complex composition, which features HBGAs,^{41,42} peptides,⁴³ and single-chain antibodies.⁴⁴

Nucleic acid aptamers are a class of 20–80 mer single-stranded DNA (ssDNA) or RNA screened from a highly diverse starting library of synthetic oligonucleotides artificially synthesized by Systematic Evolution of Ligands by Exponential Enrichment (SELEX).^{45–47} Aptamers exhibit high affinity and specificity for target molecules; are easy to prepare, label and modify; have good levels of stability, and are cost effective.^{48–51} Over recent years, a large range of nucleic acid aptamers targeting specific viruses, antibiotics and small molecules have been identified and applied to clinical diagnosis and therapy.^{52–54} Previous studies have reported aptamers against different norovirus targets, including VLPs, the P domain, and VPg.^{55–60} These previous studies mainly focused on investigating the affinity of aptamers to their targets, but did not explore their potential ability to neutralize HuNoV infections, largely due to limitations in evaluation methodology. In vitro ligand-binding blocking methods are difficult to simulate the real cell environment, and real animal models are expensive and difficult to perform in many laboratories. However, previous studies by Qiao⁶¹ and Kimura⁶² reported a splitting NanoLuc luciferase (Nluc)-based surrogate infection/neutralization assay against HuNoV in 2022, thus making it possible to investigate the efficacy of inhibitors against HuNoVs at the cellular level.

In the present study, we generated nucleic acid aptamers against HuNoV GII.4 and GII.17 VLPs by SELEX screening and verified their affinity and specificity by BioLayer interferometry, dot blotting, and enzyme linked aptamer sorbent assay (ELASA). In addition, we validated the potential ability of these candidate aptamers to neutralize HuNoVs infection by VLP/PGM binding blockade assays (in vitro) and at the cellular level by split Nluc-based surrogate infection/neutralization assays.

Materials and Methods

Cells, Plasmids, Antibodies and VLPs

SF9 (insect ovary) cells, 293T (Human embryonic kidney) and Caco2 (human colorectal adenocarcinoma) cells were obtained from Chinese Academy of Sciences Cell Bank (Shanghai, China). SF9 cells were cultured in Sf-900 II SFM (Gibco) at 28°C to express HuNoV VLPs. The VP1 fragments of HuNoV GII.4 strain Hu/GII.4/DBM15-156/2015 (GenBank ID: MG786781.1) and HuNoV GII.17 strain Hu/GII.P17_GII.17/KR/2015 (GenBank ID: 38168209) were inserted into the pFastBac1 plasmid (Thermo Fisher Scientific, Waltham, MA) to generate HuNoV GII.4 VLP and HuNoV GII.17 VLP by the Bac-to-Bac baculovirus expression system. To generate HiBiT-VLPs, we introduced the HiBiT tag (VSGWRLFKKIS) into the N-terminus of the HuNoV VP1 fragment by point mutation and used the same expression system as described above. The obtained VLPs/HiBiT-VLPs were negatively stained with 2% aqueous uranyl acetate and morphologically analyzed by transmission electron microscopy (TEM) (JEM-1400Flash, JEOL, Japan). The generation of VLPs was verified by Western blotting (WB) with previously prepared rabbit anti-GII.4 VLP and rabbit anti-GII.17 VLP polyclonal antibodies, and fusion of the HiBiT tag was verified by Nano-Glo HiBiT blotting (Promega, Madison, WI). We used the same method to generate a series of HuNoV VLPs and corresponding HiBiT VLPs: GII.4 New Orleans (GenBank ID: LC177654.1), GII.4 Sydney (GenBank ID: KR904228.1), GI.3 (GenBank ID: MZ021600.1), GII.2 (GenBank ID: NC_039476.1), GII.3 (GenBank ID: KY442319.1), GII.6 (GenBank ID: LC790056.1). When constructing pFastBac1 plasmids containing these HuNoV VP1 sequences, a His tag was inserted into the C-terminus of the VP1 sequence, and detection of these VLPs and HiBiT VLPs were carried out by WB (anti-His monoclonal antibody) and HiBiT blotting. The obtained VLPs were diluted with phosphate buffered saline (PBS) and stored at –80°C to await experimentation.

To generate 293T cells that were able to stably express LgBiT protein, we inserted the LgBiT gene into the pCDH-CMV-MCS-EF1-Puro plasmid, thus generating LgBiT-pCDH-CMV-MCS-EF1-Puro. Then, 293T cells were transfected with LgBiT-pCDH-CMV-MCS-EF1-Puro, psPAX2, and pMD2.G. After two days, the supernatant was harvested,

centrifuged at 12,000 rpm for 5 min and filtered through a 0.22 μm syringe filter to generate a lentiviral vector encoding LgBiT. Two days after infection with the lentiviral vector, 293T cells were maintained in Dulbecco's modified Eagle's medium (DMEM) (Gibco) with 10% fetal bovine serum (FBS) (Gibco) and 2 $\mu\text{g}/\text{mL}$ of puromycin, thus generating 293T-LgBiT cells. qRT-PCR and the $2^{-\Delta\Delta\text{Ct}}$ method⁶³ were used to detect the relative expression of LgBiT mRNA in 293T-LgBiT cells; primer information (β -actinF, β -actinR, LgBiTF, LgBiTR) is provided in [Supplemental Table 1](#).⁶¹ WB was used to detect the expression of LgBiT protein in cells; for this, we purchased an anti-LgBiT monoclonal antibody (mAb) from Promega (Cat# N7100).

Selection of Aptamers by SELEX

The ssDNA library consisted of constant region on both sides (5'-CAGGGGGACGCACCAAGG-(N)₄₀-ATCACGCAGCACGCGGGGTCATGG-3') with a 42mer random region in the middle, which was synthesized by Shengong (Shanghai, China). We labelled the target protein (HuNoV GII.4 and GII.17 VLPs) with Biotin using a Thermo Scientific™ EZ-Link™ NHS-PEG4-Biotin kit. Then, the magnetic particles coupled with the target protein were added to a micro-library and incubated at room temperature for 90 min. After rotation and mixing, 50% of the total volume was aspirated into two 1.5 mL tubes and adsorbed onto magnetic racks for 1–2 min. Each tube was washed with 0.5–1.0 mL of Buffer-A (PBSTM, 1 \times PBS, 1 mm MgCl₂, 0.05% Tween 20) until the wash solution became clear and did not contain unbound aptamer microbeads. The two tubes of beads were then mixed and washed twice with 500 μL of Buffer-B (PBSTM, 1X PBS, 1 mm MgCl₂, 0.05% (V/V) Tween 20, 2 mg/mL bovine serum albumin (BSA)). Finally, the tubes were re-centrifuged with 50 μL of Buffer-B.

The aptamers obtained were separated from the magnetic particles by NaOH and Tris-Cl. The aptamers were then desalted with an equilibrium filtration column, and the resulting filtrate was subjected to PCR amplification and 8–10% non-denaturing polyacrylamide electrophoresis. Following separation, the gel was recovered and ssDNA was concentrated using isopropanol to be used as a secondary library for the next round of screening.

We performed 10 rounds of positive sieving for HuNoV GII.4 and GII.17 VLPs, respectively. Finally, the initial fluid from round 1 and the fluid from the final round were taken for high-throughput unidirectionally sequenced using Illumina Miseq. Next, the data arising from forward sequencing were cut using cutadapt v1.12 to retain only the middle portion of the sequences. Secondary structure folding analysis and ΔG prediction for the candidate aptamer sequences were performed with the DNA Mfold online server (<http://mfold.rna.albany.edu/>).⁶⁴

Aptamer-Mediated Dot-Blotting

HuNoV GII.4 VLP and HuNoV GII.17 VLP were diluted with PBS to a range of concentrations (0.5 mg/mL, 0.25 mg/mL, 0.125 mg/mL, and 0.0625 mg/mL) and then 2 μL of each was spotted onto a nitrocellulose membrane (pore size: 0.45 μm ; Fisher Scientific Suwanee, GA, USA). For specificity validation experiments, a series of control solutions (PGM, *E. coli* lysate, Caco2 lysate, EV71, coronavirus S protein, and astrovirus) were diluted to 0.5 mg/mL with PBS, and PBS was used as a negative control. The membrane was left at room temperature for 40 min to dry and then were immersed in phosphate buffered saline with Tween 20 (PBST) solution containing 5% Bovine Serum Albumin (BSA), incubated at room temperature for 30 min, and then washed three times with PBST (5 min per wash). Cy5-labelled aptamers were diluted to 100 nM with PBST and the membrane was placed in aptamer solution, and incubated at 37°C in the dark. Following 1 h of incubation, the membrane was washed five times with PBST (5 min per wash). Finally, the membrane was removed and immediately analyzed for fluorescence with a multifunctional biomolecular laser imaging system (Typhoon 9500, USA).

Determination of Dissociation Constants

Binding affinities between aptamers and GII.4/GII.17 VLPs were determined by the BioLayer Interferometry (BLI) technique. HuNoVs VLPs were first formulated into 300nM (for GII.4 VLP), 150 nM, 75 nM, 37.5 nM and 18.75 nM (for GII.17 VLP) solutions and candidate biotin-labelled aptamers were diluted to 100 nM with binding buffer (PBST + 5 mm Mg²⁺). The SA biosensors, modified with streptavidin, were placed in pre-wetted buffer (PBS + 5 mm Mg²⁺) and soaked for 10 min. Next, PBST (for baseline equilibrium, "Baseline 1"), 100 nM bio-Aptamer (for binding, "loading"),

PBST (for baseline equilibrium, “Baseline 2”), different concentrations of protein solution (for aptamer-protein binding, “association”), and PBST (for dissociation, “dissociation”) were added sequentially to a black 96-well plate.

Affinity assay experiments were then performed using the Molecular Interactor Fortebio Octet RED96 (USA), and the analysis steps were set up in the instrument software: “Baseline 1” was set up for 60s; “Loading” was set up for 300 s; “Baseline 2” was set up for 300 s; “Association” was set up for 900 s, and “Dissociation” was set up for 900 s. The assay was performed at an analytical speed of 1000 rpm and an assay temperature of 37°C. All data were acquired in Fortebio Data Acquisition 6.4 and analyzed in Fortebio Data Analysis 6.4 to determine the binding dissociation constant K_d . The binding and dissociation curves were aligned, and a 1:1 model was selected for global curve fitting to perform the process that yielded in the binding dissociation constant K_d .

ELASA

The ELASA was performed in a manner that was similar to the ELISA method.^{43,65} In this particular experiment, antibodies were replaced with biotin-labelled aptamers. HuNoV GII.4 and GII.17 VLPs were first diluted to an appropriate concentration with inclusion buffer (Shenggong, Shanghai, China). Then, 100 μ L of diluted VLPs solution was added to each well of a flat-bottomed polystyrene 96-well plate and left overnight at 4°C to allow coating. After three washes with 300 μ L of PBST, 100 μ L of PBST containing 5% skimmed milk and 10 nM of a mixture of unrelated DNA oligonucleotides [*Listeria monocytogenes* primers hlyQF/R and L23SQF/R] ([Supplemental Table 1](#))⁶⁶ was added to each well and left at 37°C for 1 h. Similarly, after three washes with PBST, 100 μ L of biotinylated aptamers was added to each well and incubated for 1 h at 37°C. After removing excess aptamers, the wells were washed three times with PBST, and 100 μ L of ELISA-grade rabbit anti-biotin-horse radish peroxidase (HRP) labelled antibody (1:5000) (Shenggong, Shanghai, China) was added to each well and incubated for 1 h at 37°C, followed by three more washes. Next, 100 μ L of 3,3',5,5'-tetramethylbenzidine (TMB) peroxidase substrate was added to each well. After 10 min at 37°C, the reaction was stopped by adding 50 μ L of 1 M phosphate. Then, we measured the absorbance at 450 nm with a microtiter plate instrument (BioTek Epoch, USA). The negative control did not feature a VLP coating on the plates, and the affinity of the aptamer was determined by the ratio of the optical density (OD) value of the test group to the OD value of the negative control (T/N ratios). In accordance with a previous study,⁶⁷ T/N ratios <2.0 were considered to indicate low or no binding (-); ratios between 2.0 and 5.0 were considered to indicate low binding (\pm); ratios between 5.0 and 10.0 were considered to indicate moderate binding (+); and ratios >10.0 were considered to indicate strong binding (++)

VLP/PGM Binding Blockade Assays

Pretreated PGM III (SIGMA, Japan) was first diluted to 2.5 mg/mL with PBS and then 100 μ L was added to each well of a flat-bottomed polystyrene 96-well plate. After coating overnight at 4°C and three washes with PBST, 100 μ L of PBST containing 5% BSA was added to each well and incubated at 37°C for 1 h. Next, 100 μ L of 10 μ g/mL HuNoV VLPs only/HuNoV VLPs + aptamers (bound 1 h ahead at 37°C) was added to each well and incubated at 37°C for 1 h to allow VLPs binding. Then, we added 100 μ L of rabbit anti-VLP antibody (1:2000) and HRP-conjugated anti-rabbit IgG (1:5000) per well sequentially and incubated at 37°C for 1 h. After five washes, 100 μ L of 3,3',5,5'-TMB peroxidase substrate was added and the reaction terminated by 50 μ L of 1 M phosphoric acid. A microtiter plate instrument was used to measure the absorbance at 450 nm. A negative control was generated by replacing VLPs with PBS although antibodies were added in the same manner as for the experimental group. Data were expressed as the blocked percentage of VLPs binding to PGM III by the aptamers.

HiBiT-VLP Internalization Inhibition Assays

As described previously,⁶¹ 3×10^4 293T-LgBiT cells were seeded per well into 96-well plates and incubated overnight at 37°C. The following day, cells were placed at 4°C for 1 h; then, the medium was removed and washed once with PBS. Next, 100 μ L of Opti-MEM/Opti-MEM + HuNoV VLPs (1.5 μ g/mL)/Opti-MEM + HuNoV VLPs (1.5 μ g/mL) + aptamers (bound previously for 1 h at 37°C) were added into each well, respectively, and then incubated at 4°C for 1 h. After washing with PBS, Opti-MEM containing NanoGlo Live Cell Substrate (Promega) was added to each well and

incubated at 37°C for 1h. A GloMax[®] 20/20 Luminometer (Promega, USA) was used to measure the cellular luciferase signal.

Cell Viability Assays

To investigate the effect of aptamers on cell viability, we treated cells with different concentrations of aptamers for 24 h and assayed the lactate dehydrogenase (LDH) activity exhibited by cells using a Cytotoxicity LDH Assay Kit-WST (DOJINDO, Japan). In brief, 3×10^4 293T-LgBiT or Caco2 cells were seeded into each well of a 96-well plate one day before the experiment. Then, the medium was removed and fresh medium/medium + aptamer was added. In addition, we set up corresponding controls in accordance with the manufacturer's instructions; 24 h later, 100 μ L of working solution was added to each well (10 μ L of lysis buffer was added in advance to the positive control wells and incubated for 30 min). The samples were then incubated for 30 min at room temperature in the dark and the reaction was then stopped by adding 50 μ L of stop solution. Immediately thereafter, the absorbance at 490 nm was measured with a microplate reader and the results were expressed as follows: cell activity rate = 1 - cell damage rate (%).

Statistical Analysis

Statistical analysis of the data was performed using GraphPad Prism version 9. Experimental data were compared between two groups with *t*-tests. When different concentrations of aptamers were involved, we used one-way analysis of variance (ANOVA) to analyze differences between each concentration and the control group. Statistically significant differences are indicated by **P* < 0.05; ***P* < 0.01; ****P* < 0.001; *****P* < 0.0001.

Results

Screening of Aptamers

After 10 rounds of screening, 10522372 and 1348564 valid sequences were obtained for HuNoV GII.4 and GII.17 VLPs, respectively. High-throughput unidirectional sequencing of these sequences revealed a high number of repetitive but valid sequences; [Supplemental Table 2](#) lists the top 50 occurrences of screened sequences for HuNoV GII.4 and GII.17 VLPs and their base counts. Most of these sequences were 40–45 bases in length, although a few of sequences were less than 30 bases in length. Eight valid sequences were selected based on the number of occurrences for subsequent experiments, and Δ G prediction for these candidate aptamers was performed using the DNA Mfold online server. Analysis revealed that the Δ G values for the eight aptamers against HuNoV GII.4 VLP ranged from -5.55 to -11.99 , while the Δ G values of the eight aptamers against HuNoV GII.17 VLP ranged from -2.85 to -13.64 ([Table 1](#)). Generally, a lower Δ G value indicates that a given aptamer has a more stable secondary structure.

Selection of ssDNA Aptamer Candidates

First, we used the DNA Mfold online server to predict the secondary structure of aptamers targeting HuNoV GII.4 and GII.17 VLPs ([Figure 1A and B](#) and [Supplemental Figure 1](#)). Sequence comparison of the aptamers was also performed to look for a commonly occurring stem-loop structure, which needs to satisfy the number of bases greater than or equal to six and appear in all eight candidate aptamers, and we found 1–3 varied in size stem loop structures in these aptamers. Next, we used Snappgene to analyze aptamer sequences and identified some common motifs (≥ 6 bases in length) that played a role in the formation of stem-loops. And we performed BioLayer interferometry (BLI) and dot blotting using these aptamers. BLI results ([Figure 1C and D](#) and [Supplemental Figure 2](#)) showed that the K_d of the four aptamers targeting the GII.4 VLP were all <100 nM, while the K_d of the other three aptamers ranged from 123 to 3380 nM. In addition, the K_d of all aptamers against GII.17 VLP were <10 nM. Dot blotting results ([Supplemental Figure 3](#)) showed that all of the aptamers against HuNoV GII.4 VLP exhibited binding to HuNoV GII.4 VLP, with a clear binding site observed at a VLP concentration of 0.25 mg/mL. For the AP4-2 aptamer, a binding site was also observed at a VLP concentration of 0.125 mg/mL. All aptamers targeting HuNoV GII.17 VLP, with the exception of AP17-3, exhibited binding to HuNoV GII.17 VLP; comparative analysis showed that AP17-4 and AP17-8 exhibited better binding to low

Table 1 Aptamer Sequences and ΔG Value Obtained for HuNoV GII.4 and GII.17 VLPs, Respectively

Name	Variable Region Sequence	ΔG
AP4-1	AACAGACGAACTGTGATAGACGAACCAAGGAAGTGAGC	-6.78
AP4-2	AACACGACAACCCTGTGACCAACGAACCACACCAAAGTGGGC	-8.31
AP4-3	AACACGACCCACGTTTCGCCTCCCACAGCCCATCAATGTGGGC	-11.01
AP4-4	AACACGACATACCTGTGCGAGACACAGACCACCAAGGTGGGC	-11.99
AP4-5	AAGCCACGCGCCGTTTCGCCAGCCACAGCCACCAATGTCGTG	-5.55
AP4-6	AAGCCACATCGCTGTGACCACCGAACCCACACCCGTCGTG	-6.62
AP4-7	AACACGACGCACCTGTGTTGGACGAACCACAAGCCTGTCTTG	-8.56
AP4-8	AACACGACAGTCGTTTCGGGAGTACAGCCATACAGTCGTG	-11.23
API7-1	AAGCCCACTTCGCTGGATTCACGAACTCCAGCAGAGTCGTG	-10.79
API7-2	GGGGGAAGCCCCACGTTTCGAAGGCCACAGTACGGGGATGTGGGC	-12.41
API7-3	GGACAGCGAACTATGAGCTTGTGGAC	-2.85
API7-4	GGAACACGACCCGTCGTG GCCATCACAGTACAGCATCGTCGTG	-13.64
API7-5	AACACGACTGAGCTCTGAAAGACGAACGTCACTGAAGTCGTG	-11.51
API7-6	CACGACCGATGTTTCGAGCAACGAACTACGCCAATGTGGGC	-10.33
API7-7	GGAAGCCCACACTTCTGTGGCCAACACAGGACATGGTGGTCGTG	-10.68
API7-8	GGAAGCCCACCTACCTGTGGAAGGTCAAACCTCACGGACGTCGTG	-11.29

concentrations of VLP. Combining these key results (ΔG , K_d and dot blotting), we selected AP4-2 and AP17-4 for subsequent experiments.

Characterization of Aptamer Affinity

ELASA is similar to ELISA except that the antibody-binding antigen was replaced with biotin labelled aptamers (Figure 2A). Different concentrations of HuNoV GII.4 VLP and HuNoV GII.17 VLP were pre-coated on plates, and

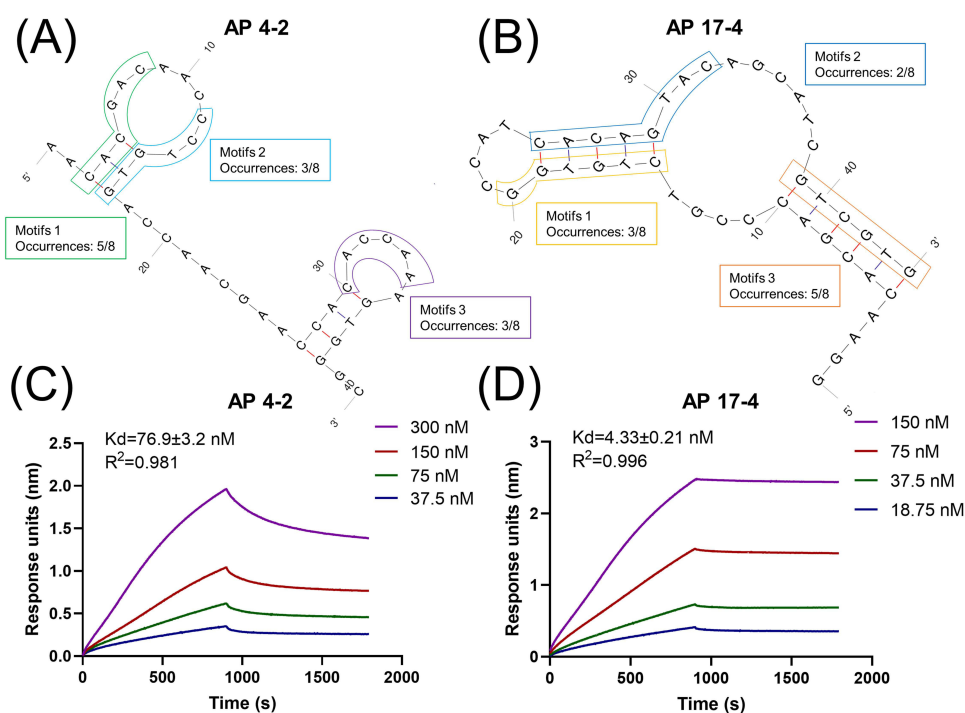


Figure 1 Secondary structure prediction and K_d values of candidate aptamers AP4-2 and AP17-4. Secondary structure prediction of (A) AP4-2 and (B) AP17-4, some common motifs (≥ 6 bases in length) occurring in the aptamers for HuNoV GII.4 and GII.17 VLPs are marked by different colored boxes and the number of occurrences is listed. Binding and dissociation curves and K_d values of (C) AP4-2 and (D) AP17-4.

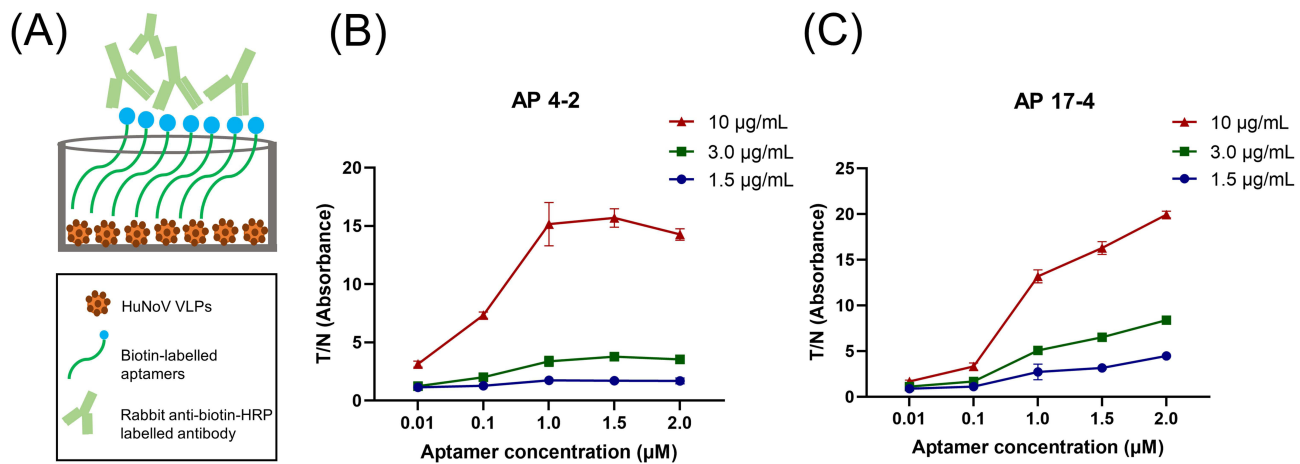


Figure 2 Affinity analysis of aptamers for targets. (A) ELASA schematic diagram. T/N of (B) AP4-2 and (C) AP17-4 at different HuNoV GII.4 and GII.17 VLP concentrations (1.5 µg/mL, 3.0 µg/mL and 10 µg/mL) and different aptamer concentrations (0.01 µM, 0.1 µM, 1.0 µM, 1.5 µM and 2.0 µM). The data are reported as means ± SEM of triplicate wells.

experiments were performed with different concentrations of biotin-labelled AP4-2 and AP17-4, respectively. As shown in Figure 2B and C, when the concentration of coated VLPs increased and the aptamer concentration remains the same, the T/N of AP4-2 and AP17-4 increased consequentially. When the concentration of encapsulated VLPs was fixed, for AP4-2, the T/N ratio gradually increased with increasing aptamer concentration and peaked at a concentration of 1.0 µM, thus indicating saturation. For AP17-4, the T/N ratio increased with increasing aptamer concentration and did not plateau even at an aptamer concentration of 2.0 µM.

Characterization of Aptamer Specificity

The specificity of AP4-2 and AP17-4 was verified by dot blotting and ELASA. As shown in Figure 3A–D, Cy5-labelled AP4-2 efficiently bound HuNoV GII.4 VLP on nitrocellulose membranes at a concentration of 0.125 mg/mL. The detection limit for AP17-4 was even lower at 0.0625 mg/mL of HuNoV GII.17 VLP. Meanwhile, AP17-4 showed weak binding to the Caco2 cell lysate, comparable to a binding strength of 0.125 mg/mL of HuNoV GII.17 VLP, although much lower than that of 0.25 mg/mL of HuNoV GII.17 VLP. Similar to the dot blotting results, the results derived from ELASA (Figure 3E and F) showed that the T/N was 3–4 for both AP4-2 and AP17-4, whereas the T/N of the four other pathogens (*E. coli*, EV71, coronavirus S protein, and astrovirus) was close to 1, thus indicating that AP4-2 and AP17-4 did not/almost did not react with these diarrhea-inducing pathogens ($P < 0.0001$). Collectively, these results show that these two aptamers exhibited excellent specificity.

Aptamer-Mediated VLP/PGM Binding Blockade

As shown in Figure 4, as the concentration of AP4-2 and AP17-4 increased, the HuNoV GII.4 and GII.17 VLPs bound to the PGM encapsulated on the bottom of the plate decreased accordingly. When the concentration of AP4-2 reached 2.5 µM, it blocked approximately 70% of the HuNoV GII.4 VLP binding to PGM; the same concentration of AP17-4 blocked approximately 40% of the HuNoV GII.17 VLP. This indicates that the two aptamers are both able to block the binding of HuNoV VLPs to the receptor *in vitro*.

Aptamer-Mediated Inhibition of VLP Internalization

As shown in Figure 5A, unlabeled GII.4 VLP, GII.17 VLP and newly generated HiBiT GII.4 VLP and HiBiT GII.17 VLP were all recognized by the antibody, and bands for HiBiT GII.4 VLP, HiBiT GII.17 VLP were slightly higher due to successful fusion with HiBiT. HiBiT blotting revealed that only HiBiT GII.4 VLP and HiBiT GII.17 VLP were recognized, and that these bands were located at the same molecular size as HuNoV VLPs (~57 kDa) (Figure 5B). TEM analysis further showed that GII.4 VLP, HiBiT GII.4 VLP (Figure 5C) and GII.17 VLP, and HiBiT GII.17 VLP

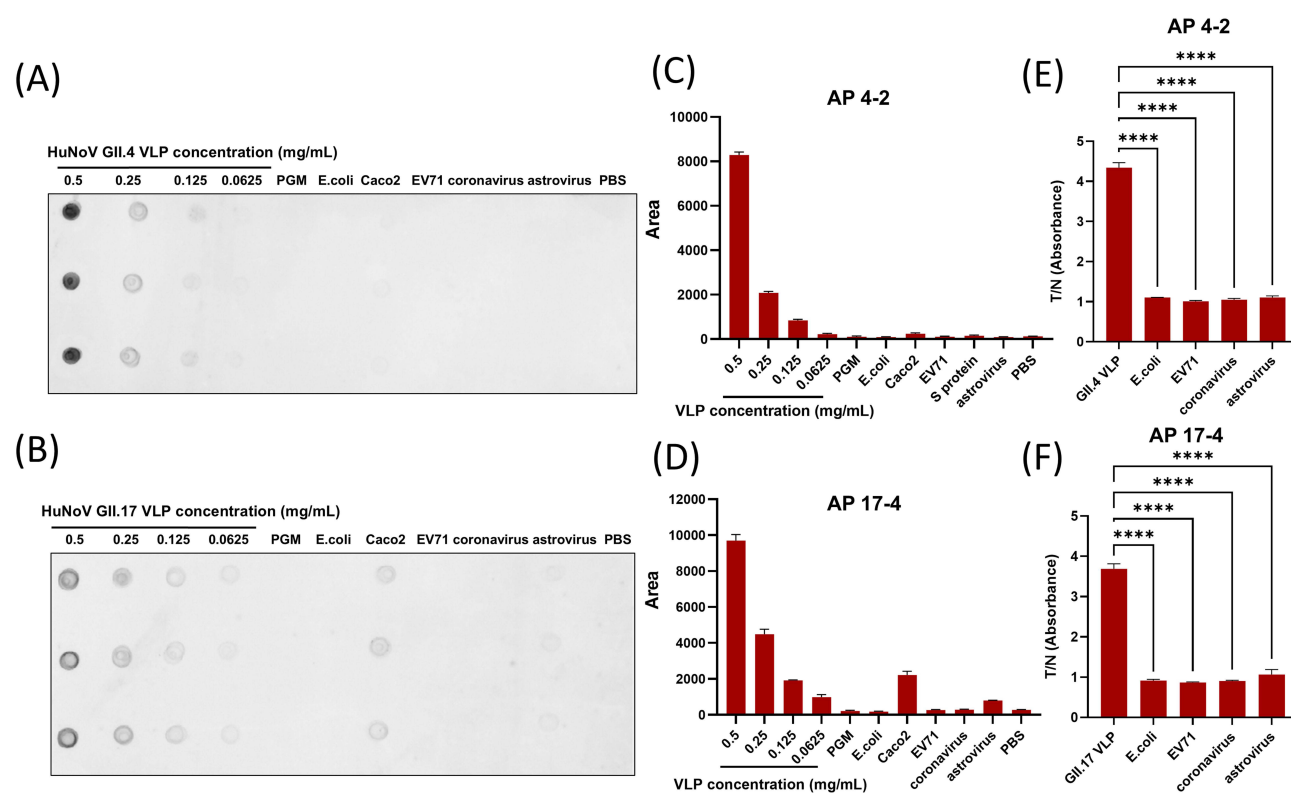


Figure 3 Specificity analysis of aptamers for targets. Dot blotting results of (A) AP4-2 and (B) AP17-4 for target HuNoV VLPs versus other unrelated pathogens/proteins. Datametric rendering of dot blotting points of (C) AP4-2 and (D) AP17-4 using ImageJ. Comparison of T/N of (E) AP4-2 and (F) AP17-4 to target HuNoV VLPs versus unrelated viruses/proteins using ELASA (****, $P < 0.0001$). The data are reported as means \pm SEM of triplicate wells.

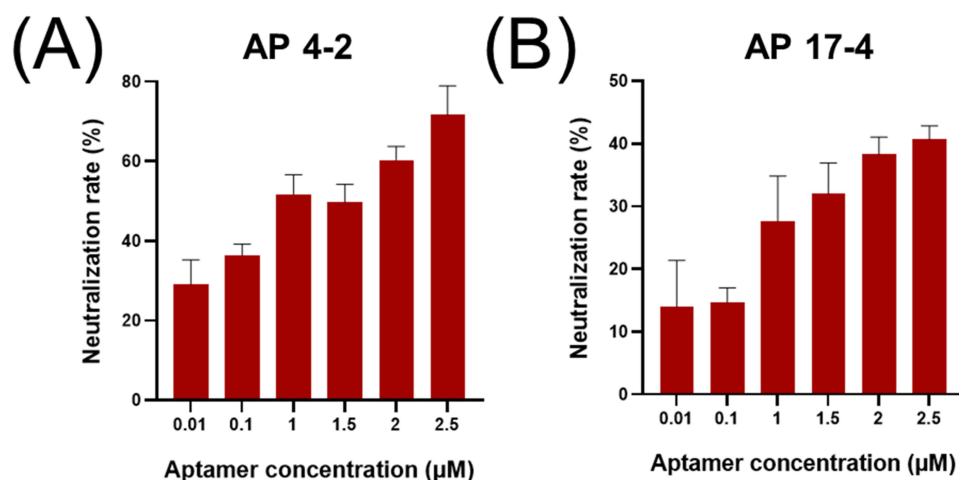


Figure 4 The capacity of blocking interaction between HuNoV VLPs and PGM III of (A) AP4-2 and (B) AP17-4 by ELISA. The data are reported as means \pm SEM of triplicate wells.

(Figure 5D) were all spherical particles with a diameter of 40–45 nm, thus demonstrating that the introduction of HiBiT had no effect on the assembly of the HuNoV VLPs.⁶¹ qRT-PCR (Figure 5E) and WB (Figure 5F) results confirmed the expression of LgBiT in 293T cells at the gene and protein levels.

To investigate whether AP4-2 and AP17-4 could reduce VLPs binding or enter 293T-LgBiT cells by pre-binding to HiBiT GII.4 VLP and HiBiT GII.17 VLP, we first bound different concentrations of the aptamers to corresponding VLPs at 37°C for 1 hour, and then inoculated the mixtures into pre-cooled 293T-LgBiT cells which were then incubated at 4°C

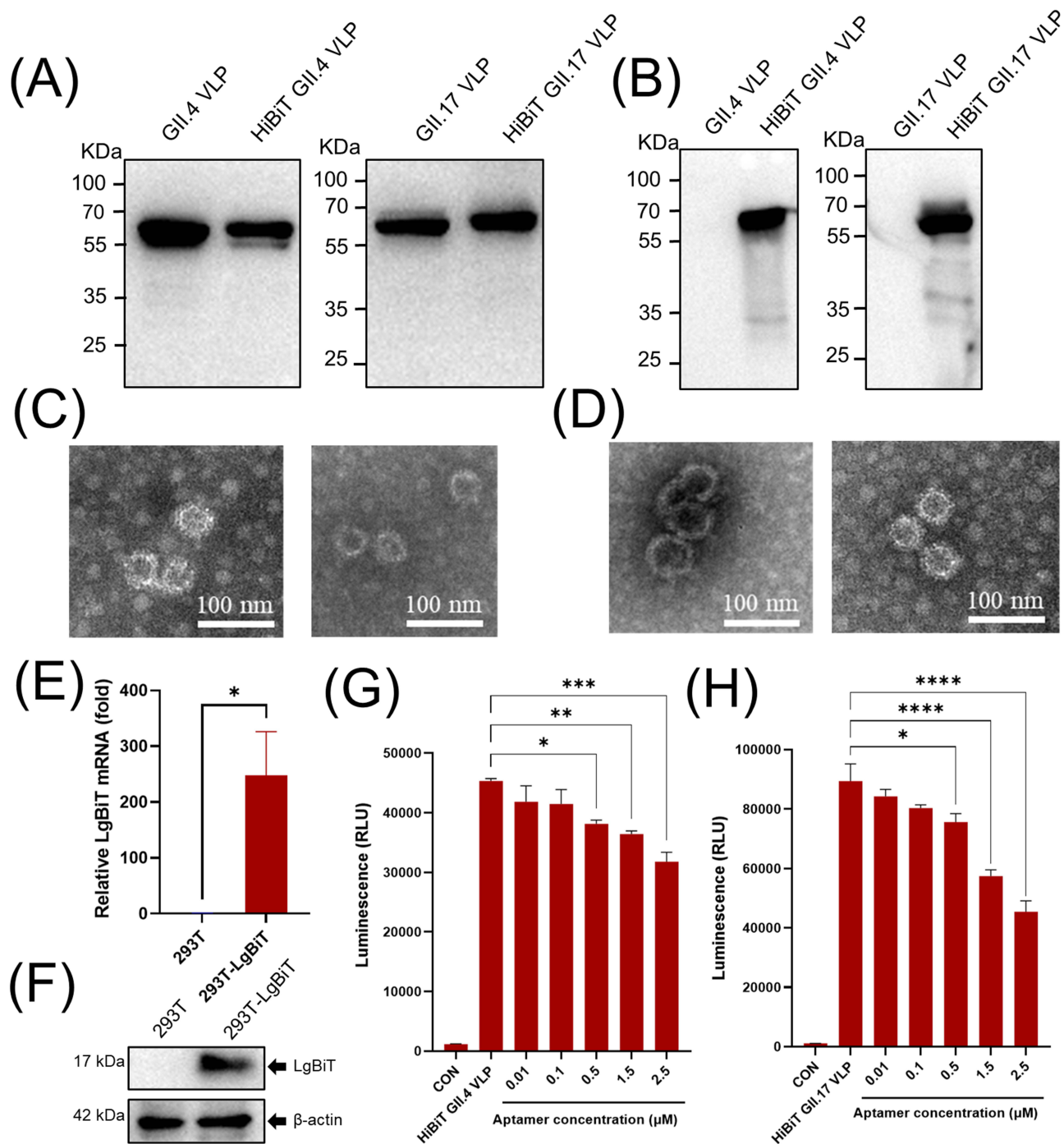


Figure 5 Generation of HuNoV HiBiT VLPs, 293T-LgBiT cell, and probing the blocking function of aptamers on VLPs internalised cells. **(A)** WB of GII.4 VLP, HiBiT GII.4 VLP, GII.17 VLP, HiBiT GII.17 VLP using polyclonal antibodies against HuNoV GII.4 VLP and HuNoV GII.17 VLP. **(B)** HiBiT blotting of GII.4 VLP, HiBiT GII.4 VLP, GII.17 VLP, HiBiT GII.17 VLP. **(C)** TEM of GII.4 VLP (left), HiBiT GII.4 VLP (right) and **(D)** GII.17 VLP (left), HiBiT GII.17 VLP (right). **(E)** mRNA expression levels of LgBiT relative to β -actin in 293T and 293T-LgBiT cells were determined by qRT-PCR. **(F)** LgBiT expression levels in 293T and 293T-LgBiT cells were detected by WB with anti-LgBiT antibody, β -actin served as an internal control. Effects of **(G)** AP4-2 and **(H)** API7-4 on HuNoV GII.4 and GII.17 VLPs cell internalisation. The data in the bar graphs are reported as means \pm SEM of triplicate wells (* $0.01 \leq P < 0.05$; ** $P < 0.01$; *** $P < 0.001$; **** $P < 0.0001$).

for 1 h to allow the VLPs to attach to the cell surface. PBS-washed cells were then left at room temperature for 1 h to allow the entry of VLPs. Subsequently, the cells were re-washed with PBS and a Nano-Glo live cell substrate was added and incubated for 1 h to detect Nluc activity. As shown in Figures 5G and H, no HiBiT VLPs were added to the cells in the blank control group; therefore, fluorescence values were very low after adding the Nano-Glo live cell substrate. The

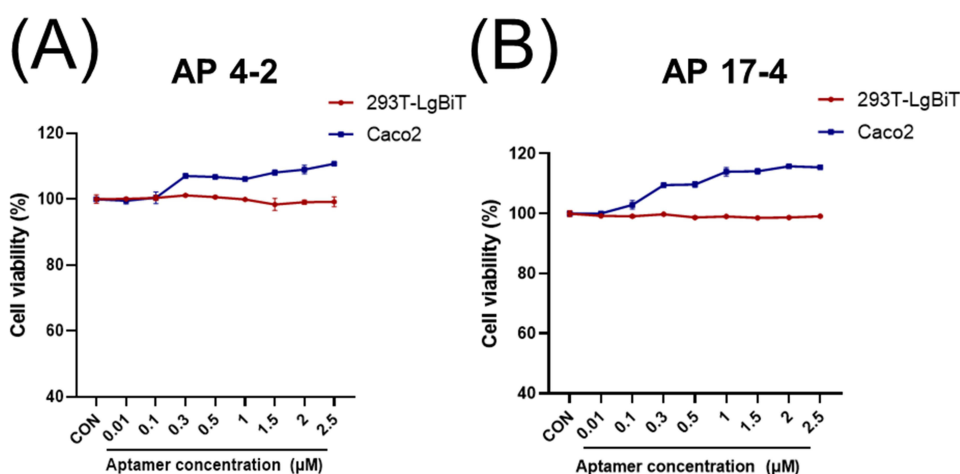


Figure 6 Effect of aptamers on cell viability. Effect of treatment of 293T-LgBiT and Caco2 cells with (A) AP4-2 and (B) AP17-4 for one day on viability as determined by cytotoxicity LDH assay. The data are reported as means \pm SEM of triplicate wells.

two groups featuring HiBiT VLPs without aptamers had fluorescence values of $4.5\text{--}8.5 \times 10^4$, respectively, thus demonstrating that HiBiT-VLPs successfully attached and entered 293T-LgBiT cells and interacted with LgBiT protein. Following the addition of aptamers, the luciferase signals arising from both groups reduced as the aptamer concentration was increased; furthermore, both groups showed a significant difference from the positive control group at an aptamer concentration of $0.5 \mu\text{M}$ ($P < 0.05$). At the highest aptamer concentration ($2.5 \mu\text{M}$), AP4-2 reduced the fluorescence value by 30% while AP17-4 reduced the fluorescence value by 49%. Collectively, these results indicate that AP4-2 and AP17-4 bound effectively to HiBiT GII.4 VLP and HiBiT GII.17 VLP and inhibit the binding or entry of VLPs into cells.

To investigate whether aptamers in this study were spectrally responsive, we expressed a series of HuNoV VLPs and HiBiT HuNoV VLPs, including two strains of GII.4: GII.4 New Orleans and GII.4 Sydney, and GII.2, GII.3, and GII.6: which have been common in recent years, and GI genome group represented by the GI.3 (Supplemental Figure 4A and B). Dot blotting showed that AP4-2 and AP17-4 bound to HuNoV VLPs of these genotypes (Supplemental Figure 4C). Meanwhile, AP4-2 and AP17-4 showed a significant inhibitory effect on the binding and internalization of all tested HiBiT HuNoV VLPs (Supplemental Figure 4D and E).

In order to exclude the toxic effect of high concentrations of aptamers on cells and the potential for cell death and a consequential reduction in fluorescence values, we next determined the viability of 293T-LgBiT cells and Caco2 after 1 day of treatment with different concentrations of AP4-2 or AP17-4. Analysis showed that even the highest aptamer concentration had no negative effect on cell viability (Figure 6A and B), thus indicating that both AP4-2 or AP17-4 were harmless to cells.

Discussion

Nucleic acid aptamers are known as chemical antibodies and play an important role in the diagnosis and treatment of many diseases.⁴⁸ Previous studies have generated aptamers against certain genotypes of HuNoVs and murine norovirus (MNV) by screening against different targets. Similar to other studies, we generated aptamers combining HuNoV GII.4 and GII.17 VLPs by the SELEX method and introduced multiple screens to identify the nucleotide sequence with the best binding ability. We chose HuNoV GII.4 because this is the most widely spread genotype globally.⁶⁸ In addition, unlike other studies, we screened and characterized aptamers for HuNoV GII.17, which is new but widespread in Asia. Furthermore, we evaluated the ability of the candidate aptamers to block VLPs binding on putative receptors and cells, and found that the number of bound VLPs decreased significantly with increasing aptamer concentration, thus implying that these aptamers may be able to block the infection process for HuNoVs.

As the number of sieving rounds increased, the number of nucleic acid aptamer sequences bound to the target VLPs decreased and the binding rate increased. Finally, we generated eight aptamers against HuNoV GII.4 and GII.17 VLPs.

Sequence analysis against the aptamers revealed a number of common motifs that are widely present in the aptamers targeting GII.4 VLP. These motifs are involved in constituting important stem-loop structures that are important for the implementation of aptamer functionality, including tight binding to the target.⁶⁹ We compared the sequences of AP4-2 and AP17-4 with previously published aptamers against noroviruses that target whole viruses, VP1 and P domain, respectively (Supplemental Table 3), and found that the aptamers we obtained did not share motifs (≥ 5 bases in length) with these aptamers (Supplemental Figure 5). We also performed ELASA against GII.4 VLP and GII.17 VLP by combining AP4-2 and AP17-4 with some of the published aptamers and found that the aptamers we obtained had similar or better affinity (date not shown).

The ΔG of these aptamers ranged from -5.55 to -13.64 , similar to those previously reported for aptamers against norovirus, with the exception of AP17-3, probably due to the inability of its apparently small number of bases to form a stable secondary structure. BLI and dot blotting revealed a strong capacity for these aptamers to bind to VLPs. The K_d of the four aptamers for GII.4 VLP were all <100 nM while the K_d of all aptamers for GII.17 VLP were all <10 nM. When considering FDA-approved aptamers, the K_d for Pegaptanib ranged from 49 to 130 pM,⁷⁰ the K_d for thrombin-binding aptamer ranged from 25 to 200 nM,⁷¹ and the K_d for adenosine/ATP aptamer was approximately 6 μM ;⁷² compared to these previously described aptamers, our aptamers exhibited a high level of target affinity. The K_d of the published aptamers against norovirus are generally in the range of tens to hundreds nM, thus AP4-2 and AP17-4 showed comparable or stronger target affinity for the target than the published aptamers against norovirus.

As the concentration of coated VLPs increased, the T/N values for AP4-2 and AP17-4 also increased, as determined by ELASA. At a VLPs concentration of 10 $\mu\text{g/mL}$, 1.0 μM of AP4-2 and AP17-4 exhibited high binding affinity to the target VLPs. In addition, AP4-2 appeared to reach a plateau at a concentration of 1.0 μM ; further increase in concentration did not enhance the T/N value; this pattern has been reported previously.⁵⁵ AP17-4 exhibited excellent binding potential, because even when the aptamer concentration reached 1.5 or 2.0 μM , its T/N value continued to increase and did not appear to reach a plateau. This indicates that the binding ability of AP17-4 to GII.17 VLP was stronger than that of AP4-2 to GII.4 VLP, consistent with the K_d values; these findings may be caused by the force between the secondary structure of aptamer and the target.

Considering that the absence of saturation peaks for AP17-4 in ELASA may be due to non-specific binding,⁷³ and in order to explore whether these two aptamers would be specific when applied to the actual detection of HuNoVs, we conducted dot blotting with a series of other viruses/viral proteins or unrelated proteins that might interfere with our results. We found that the binding affinities of AP4-2 and AP17-4 to these interference groups were similar to the negative control, consistent with the ELASA results. However, we also found that the binding ability of AP17-4 to 0.5 mg/mL Caco2 cell lysate was comparable to that of 0.125 mg/mL GII.17 VLP; this may have been due to the complex protein composition in Caco2 cells. In other studies, when investigators used the aptamers for testing actual stool samples, other impurities in the original stool samples caused non-specific binding; thus, the original samples needed to be diluted by 100–500-fold.^{44,57}

RT-qPCR is the most commonly used technique to detect clinical samples, but as mentioned above, this method may overestimate the actual infectivity by including fragments of genes or genomes that are not included in the capsid.^{36,74} Ligand-based detection techniques can be very predictive of the amount of infectious HuNoV or MNV particles in a sample and have been used previously to investigate viral inactivation by different treatments, including ethanol, chlorine, heat, and high-pressure.^{39,40,75–77} An aptamer can exert similar characteristics to the receptor when binding to the norovirus capsid; in a previous study, Moore et al⁷⁸ compared the M6-2 aptamer for GII.4 huNoV with HBGA and a commercially available antibody against the GII gene group, and found when evaluating the effect of heat treatment on the activity of the target VLPs. Therefore, the aptamers we generated could theoretically be applied to an actual assay by binding and enriching the HuNoVs capsid in samples; this could then be followed by RT-qPCR to confirm that the amplified gene fragments are capsid-coated and infectious, thus improving the accuracy of detection.

The aptamers previously generated by Faircloth et al against Norwalk and Tulane VPg exhibited better affinity for the target and are considered to represent potential therapeutic agents as the VPg protein is involved in key functions of viral replication; however, these aptamers have yet to be validated experimentally.⁷⁹ Aptamers do have potential as a therapeutic agents when compared to antibodies or other small molecules because they are smaller and bind more

readily to the surface of target proteins, in addition to being highly stable and active over a wide temperature range.⁸⁰ More importantly, once the sequence of an aptamer has been determined, the differences between synthesized batches are likely to be almost negligible.

VLP/PGM binding blockade experiments are unavoidable when evaluating the blocking effect of an antibody against HuNoVs. Similarly, in the present study, AP4-2 and AP17-4 bound HuNoV GII.4 and GII.17 VLPs in a concentration gradient-dependent manner, thereby blocking their binding to PGM, thus suggesting that our aptamers may exhibit functionality similar to that of antibodies.

However, *in vitro* binding does not imply a potential antiviral effect. In a previous study, fucoidan and 2'-fucosyllactose were both reported to bind to the HuNoVs capsid at the same pockets with HBGA, although the results of viral suppression assays performed in zebrafish showed that only fucoidan, but not 2'-fucosyllactose, inhibited the replication of HuNoVs in zebrafish larvae.⁸¹ Some aptamers been shown to exhibit antiviral activity against other viruses, thus indicating that their activity is primarily derived from the inhibition of target protein activity.^{82–84} Some specific aptamers, such as an RNA aptamer for the RIG-I protein, can exert antiviral activity by inducing an innate immune response.⁸⁵ While not utilizing real HuNoVs, Ayyar et al⁸⁶ found that GII.4 Sysd VLP inhibited the replication of fecal isolate HuNoV GII.4 in a dose-dependent manner in intestinal organoids, thus proving the validity of HuNoV VLPs as a viral surrogate for infection modelling studies. Considering the high cost of culturing organoids, the significant handling requirements, and the possible effects of interfering factors (eg, bile acids and microorganisms) in the culture medium, we used the split Nluc-based surrogate infection/neutralization assay developed by Qiao et al⁶¹ to evaluate the infection-blocking functionality of AP4-2 and AP17-4 at the cellular level. This represents a very promising approach that requires only the insertion of an 11 amino acid HiBiT tag into the pFasrBac1 plasmid constructed to express HiBiT-VLPs. This small tag had no effect on the self-assembly and immunogenicity of VLPs. Cells were also induced to express the LgBiT protein by transient or lentiviral infection; when the HiBiT-VLPs were adsorbed and entered the cells, the HiBiT reacted with LgBiT and emitted a detectable luciferase signal upon addition of the substrate. In a previous study, Qiao et al⁶¹ reported that the neutralization of VLP-HiBiT entry of 12 mouse antisera detected by this method showed correlated well with classical VLP/PGM blockade assay. In the current study, we found that AP4-2 and AP17-4 reduced the luciferase signal of HuNoV HiBiT-VLPs in a concentration-dependent manner; we hypothesize that this effect was caused by the aptamer binding to HuNoV VLPs and inhibiting their ability to bind to the cell surface receptor.

To explain why a single aptamer can react with multiple genotypes HuNoV VLPs, we performed structural prediction and simulated docking of HuNoV GII.4 VP1 with AP4-2 and HuNoV GII.17 VP1 with AP17-4, and the results showed that both AP4-2 and AP17-4 bind at the position of the outer shell structural domain of VP1 (S-domain, consisting of 221 residues at the N-terminal), which is relative conservative during the HuNoV evolution¹ ([Supplemental Figure 6A](#) and [D](#)). We also found several possible docking sites in MOE software ([Supplemental Figure 6B](#) and [E](#)) and mutated the base of AP4-2 and AP17-4 according to previously published methodology ([Supplemental Figure 7A](#) and [B](#)).⁸⁷ The mutated aptamers were subjected to ELASA experiments. It was found that base 18(A) and base 19(C) are important for AP4-2 binding to GII.4 VLP, and mutating the bases of these sites separately resulted in a 32.01% and 34.06% decrease in affinity, respectively ([Supplementary Figure 6C](#)). The base 44(G) is important for AP17-4 binding to GII.17 VLP, and the base mutation of this site resulted in a 36.78% decrease in affinity ([Supplementary Figure 6F](#)). Notably, mutation of bases 8(G) and base 11(C) of AP17-4 respectively, both resulted in slightly increased affinity for GII.17 VLP. We performed secondary structure prediction of the aptamers after mutation of AP17-4 bases ([Supplemental Figure 8](#)). The results show that mutating base 8(G) or base 11(C) respectively does not cause significant changes in the secondary structure of aptamers, and the major stem-loop structure is retained. However, mutation of a single base of 44(G) results in a significant reduction of one of the loops and a significant lengthen in one of the stem structures of the aptamer. Stem length and ring size are vital for aptamer-binding targets.⁸⁸ We hypothesize that base 44(G) is important for maintaining the normal stem-loop structure of the aptamer, which in turn affects the binding effect to the target, in contrast to mutations on either 8(G) or 11(C), which did not cause significant changes in spatial conformation of AP17-4, and therefore had little effect on the affinity between the AP17-4 and the VP1 protein.

Furthermore, cell viability assays demonstrated that AP4-2 and AP17-4 were not toxic to cells, thus confirming the significant potential of developing AP4-2 and AP17-4 as anti-HuNoV agents. We also explored the stability of AP4-2 and

AP17-4 based on previously reported method⁸⁹ and found both AP4-2 and AP17-4 displayed good stability at 37°C in cell culture medium containing 10% FBS. According to the images of gel electrophoresis and PAGE, AP17-4 could still exhibit clear bands after 72 h of incubation, while AP4-2 showed gradual dispersion of the bands after 24 h of incubation, indicating the degradation (Supplemental Figure 9). We hypothesize that the greater stability of AP17-4 is related to its more complex secondary structure and more stem-forming base pairs,^{90,91} which is also manifested in the lower ΔG value of AP17-4 ($\Delta G = -13.64$) than AP4-2 ($\Delta G = -8.31$). The stability of aptamer can be improved by modifying the bases, such as systematically replacing the natural nucleotides with 2'-OMe or 2'-F nucleotides to generate xeno nucleic acids.⁷⁰

Conclusion

In this study, we generated two ssDNA aptamers with high affinity to HuNoV GII.4 and GII.17 VLPs. Neither of these aptamers reacted with other pathogens that may cause diarrhea or with non-relevant protein, thus providing the basis for the development of an aptamer-based detection technique for HuNoV. In addition, these aptamers blocked the binding of VLPs to PGM and effectively inhibited the attachment and internalization of VLPs into cells, thus suggesting that they could be applied against HuNoVs infections in a similar manner to other aptamers reported previously.^{92,93} We also demonstrated that both two aptamers can react with numerous genotypic subtypes HuNoV VLPs and can inhibit the binding and entry of these VLPs into cells. This is the first report of the generation of aptamers by screening with HuNoV GII.17 VLP and the first demonstration of the therapeutic efficacy of aptamers targeting HuNoVs. In future studies, we will further explore the specific sites of binding for the two aptamers and optimize the aptamer sequences with the aim of better exploiting their functions for detection and therapy.

Acknowledgments

Financial support for this research was provided by the National Science and Technology Major Project (Reference: 2018ZX10101003-005-010), the National Key Research and Development Program of China (Reference: 2021YFE0200600), and the National Natural Science Foundation of China (Reference: 21776071).

Disclosure

The authors report a patent 202110559265.5 pending to Junqi Zhang, Youhua Xie, Minjia Sun, and Jing Liu. The authors report no other conflicts of interest in this work.

References

- Prasad BVV, Hardy ME, Dokland T, Bella J, Rossmann MG, Estes MK. X-ray crystallographic structure of the Norwalk virus capsid. *Science*. 1999;286(5438):287–290. doi:10.1126/science.286.5438.287
- Vongpunasawad S, Prasad BVV, Estes MK. Norwalk virus minor capsid protein VP2 associates within the VP1 shell domain. *J Virol*. 2013;87(9):4818–4825. doi:10.1128/JVI.03508-12
- Lopman BA, Steele D, Kirkwood CD, Parashar UD. The vast and varied global burden of norovirus: prospects for prevention and control. *PLoS Med*. 2016;13(4):e1001999. doi:10.1371/journal.pmed.1001999
- Kotwal G, Cannon JL. Environmental persistence and transfer of enteric viruses. *Curr Opin Virol*. 2014;4:37–43. doi:10.1016/j.coviro.2013.12.003
- Seitz SR, Leon JS, Schwab KJ, et al. Norovirus infectivity in humans and persistence in water. *Appl Environ Microbiol*. 2011;77(19):6884–6888. doi:10.1128/AEM.05806-11
- Dolin R, Blacklow NR, DuPont H, et al. Biological properties of Norwalk agent of acute infectious nonbacterial gastroenteritis. *Proc Soc Exp Biol Med*. 1972;140(2):578–583. doi:10.3181/00379727-140-36508
- Richards GP, Watson MA, Meade GK, Hovan GL, Kingsley DH. Resilience of norovirus GII.4 to freezing and thawing: implications for virus infectivity. *Food Environ Virol*. 2012;4(4):192–197. doi:10.1007/s12560-012-9089-6
- Mathijs E, Stals A, Baert L, et al. A review of known and hypothetical transmission routes for noroviruses. *Food Environ Virol*. 2012;4(4):131–152. doi:10.1007/s12560-012-9091-z
- Siebenga JJ, Vennema H, Zheng DP, et al. Norovirus illness is a global problem: emergence and spread of norovirus GII.4 variants, 2001–2007. *J Infect Dis*. 2009;200(5):802–812. doi:10.1086/605127
- Chen SY, Chiu CH. Worldwide molecular epidemiology of norovirus infection. *Paediatr Int Child Health*. 2012;32(3):128–131. doi:10.1179/2046905512Y.0000000031
- De Graaf M, van Beek J, Vennema H, et al. Emergence of a novel GII.17 norovirus - End of the GII.4 era? *Euro Surveill*. 2015;20(26):8–15. doi:10.2807/1560-7917.ES2015.20.26.21178
- Zhang P, Chen LP, Fu Y, et al. Clinical and molecular analyses of norovirus-associated sporadic acute gastroenteritis: the emergence of GII.17 over GII.4, Huzhou, China, 2015. *Bmc Infect Dis*. 2016;16(1):717. doi:10.1186/s12879-016-2033-x

13. Lopman BA, Reacher MH, Vipond IB, Sarangi J, Brown DW. Clinical manifestation of norovirus gastroenteritis in health care settings. *Clin Infect Dis*. 2004;39(3):318–324. doi:10.1086/421948
14. Wingfield T, Gallimore CI, Xerry J, et al. Chronic norovirus infection in an HIV-positive patient with persistent diarrhoea: a novel cause. *J Clin Virol*. 2010;49(3):219–222. doi:10.1016/j.jcv.2010.07.025
15. De Clercq E, Li GD. Approved antiviral drugs over the past 50 years. *Clin Microbiol Rev*. 2016;29(3):695–747. doi:10.1128/CMR.00102-15
16. Duizer E, Schwab KJ, Neill FH, Atmar RL, Koopmans MPG, Estes MK. Laboratory efforts to cultivate noroviruses. *J Gen Virol*. 2004;85(1):79–87. doi:10.1099/vir.0.19478-0
17. Cheng C, Cai X, Li JJ, Zhang XM, Xie YH, Zhang JQ. In vitro culture of human norovirus in the last 20 years. *Biomedicines*. 2024;12(11):2442. doi:10.3390/biomedicines12112442
18. Ettayebi K, Crawford SE, Murakami K, et al. Replication of human noroviruses in stem cell-derived human enteroids. *Science*. 2016;353(6306):1387–1393. doi:10.1126/science.aaf5211
19. Sato S, Hisaie K, Kurokawa S, et al. Human norovirus propagation in human induced pluripotent stem cell-derived intestinal epithelial cells. *Cell Mol Gastroenter*. 2019;7(3):686–688.
20. Mirabelli C, Santos-Ferreira N, Gilliland MG, et al. Human norovirus efficiently replicates in differentiated 3D-human intestinal enteroids. *J Virol*. 2022;96(22):e0085522. doi:10.1128/jvi.00855-22
21. White LJ, Ball JM, Hardy ME, Tanaka TN, Kitamoto N, Estes MK. Attachment and entry of recombinant Norwalk virus capsids to cultured human and animal cell lines. *J Virol*. 1996;70(10):6589–6597. doi:10.1128/jvi.70.10.6589-6597.1996
22. Cheatham S, Souza M, McGregor R, Meulia T, Wang Q, Saif LJ. Binding patterns of human norovirus-like particles to buccal and intestinal tissues of gnotobiotic pigs in relation to A/H histo-blood group antigen expression. *J Virol*. 2007;81(7):3535–3544. doi:10.1128/JVI.01306-06
23. Lou FF, Huang PW, Neetoo H, et al. High-pressure inactivation of human norovirus virus-like particles provides evidence that the capsid of human norovirus is highly pressure resistant. *Appl Environ Microbiol*. 2012;78(15):5320–5327. doi:10.1128/AEM.00532-12
24. Nilsson J, Rydell GE, Le Pendu J, Larson G. Norwalk virus-like particles bind specifically to A, H and difucosylated Lewis but not to B histo-blood group active glycosphingolipids. *Glycoconjugate J*. 2009;26(9):1171–1180. doi:10.1007/s10719-009-9237-x
25. Souza M, Cheatham SM, Azevedo MSP, Costantini V, Saif LJ. Cytokine and antibody responses in gnotobiotic pigs after infection with human norovirus genogroup II.4 (HS66 strain). *J Virol*. 2007;81(17):9183–9192. doi:10.1128/JVI.00558-07
26. Xi JA, Min W, Graham DY, Estes MK. Expression, self-assembly, and antigenicity of the Norwalk virus capsid protein. *J Virol*. 1992;66(11):6527–6532. doi:10.1128/jvi.66.11.6527-6532.1992
27. Tan M, Zhong WM, Song D, Thornton S, Jiang X. E.coli-expressed recombinant norovirus capsid proteins maintain authentic antigenicity and receptor binding capability. *J Med Virol*. 2004;74(4):641–649. doi:10.1002/jmv.20228
28. Ma YM, Li JR. Vesicular stomatitis virus as a vector to deliver virus-like particles of human norovirus: a new vaccine candidate against an important noncultivable virus. *J Virol*. 2011;85(6):2942–2952. doi:10.1128/JVI.02332-10
29. Teunis PFM, Moe CL, Liu P, et al. Norwalk virus: how infectious is it? *J Med Virol*. 2008;80(8):1468–1476. doi:10.1002/jmv.21237
30. Atmar RL, Opekun AR, Gilger MA, et al. Determination of the 50% human infectious dose for Norwalk virus. *J Infect Dis*. 2014;209(7):1016–1022. doi:10.1093/infdis/jit620
31. Kageyama T, Shinohara M, Uchida K, et al. Coexistence of multiple genotypes, including newly identified genotypes, in outbreaks of gastroenteritis due to Norovirus in Japan. *J Clin Microbiol*. 2004;42(7):2988–2995. doi:10.1128/JCM.42.7.2988-2995.2004
32. Glowacka I, Harste G, Witthuhn J, Heim A. An improved one-step real-time reverse transcription-PCR assay for detection of norovirus. *J Clin Microbiol*. 2016;54(2):497–499. doi:10.1128/JCM.02206-15
33. Cannon JL, Barclay L, Collins NR, et al. Genetic and epidemiologic trends of norovirus outbreaks in the United States from 2013 to 2016 demonstrated emergence of novel GII. 4 recombinant viruses. *J Clin Microbiol*. 2017;55(7):2208–2221. doi:10.1128/JCM.00455-17
34. Kojima S, Kageyama T, Fukushi S, et al. Genogroup-specific PCR primers for detection of Norwalk-like viruses. *J Virol Methods*. 2002;100(1–2):107–114. doi:10.1016/S0166-0934(01)00404-9
35. Costantini V, Grenz L, Fritzing A, et al. Diagnostic accuracy and analytical sensitivity of IDEIA norovirus assay for routine screening of human norovirus. *J Clin Microbiol*. 2010;48(8):2770–2778. doi:10.1128/JCM.00654-10
36. Knight A, Li D, Uyttendaele M, Jaykus LA. A critical review of methods for detecting human noroviruses and predicting their infectivity. *Crit Rev Microbiol*. 2013;39(3):295–309. doi:10.3109/1040841X.2012.709820
37. Kele B, Lengyel G, Deak J. Comparison of an ELISA and two reverse transcription polymerase chain reaction methods for norovirus detection. *Diagn Microbiol Infect Dis*. 2011;70(4):475–478. doi:10.1016/j.diagmicrobio.2011.04.002
38. Vinjé J. Advances in laboratory methods for detection and typing of norovirus. *J Clin Microbiol*. 2015;53(2):373–381. doi:10.1128/JCM.01535-14
39. Dancho BA, Chen H, Kingsley DH. Discrimination between infectious and non-infectious human norovirus using porcine gastric mucin. *Int J Food Microbiol*. 2012;155(3):222–226. doi:10.1016/j.ijfoodmicro.2012.02.010
40. Leon JS, Kingsley DH, Montes JS, et al. Randomized, double-blinded clinical trial for human norovirus inactivation in oysters by high hydrostatic pressure processing. *Appl Environ Microbiol*. 2011;77(15):5476–5482. doi:10.1128/AEM.02801-10
41. Pan LW, Zhang QG, Li X, Tian P. Detection of human norovirus in cherry tomatoes, blueberries and vegetable salad by using a receptor-binding capture and magnetic sequestration (RBCMS) method. *Food Microbiol*. 2012;30(2):420–426. doi:10.1016/j.fm.2011.12.026
42. Tian P, Engelbrektsen A, Mandrell R. Two-log increase in sensitivity for detection of norovirus in complex samples by concentration with porcine gastric mucin conjugated to magnetic beads. *Appl Environ Microbiol*. 2008;74(14):4271–4276. doi:10.1128/AEM.00539-08
43. Rogers JD, Ajami NJ, Fryszczyn BG, Estes MK, Atmar RL, Palzkill T. Identification and characterization of a peptide affinity reagent for detection of noroviruses in clinical samples. *J Clin Microbiol*. 2013;51(6):1803–1808. doi:10.1128/JCM.00295-13
44. Huang WZ, Samanta M, Crawford SE, et al. Identification of human single-chain antibodies with broad reactivity for noroviruses. *Protein Eng Des Sel*. 2014;27(10):339–349. doi:10.1093/protein/gzu023
45. Tuerk C, Gold L. Systematic evolution of ligands by exponential enrichment: RNA ligands to bacteriophage T4 DNA polymerase. *Science*. 1990;249(4968):505–510. doi:10.1126/science.2200121
46. Ellington AD, Szostak JW. In vitro selection of RNA molecules that bind specific ligands. *Nature*. 1990;346(6287):818–822. doi:10.1038/346818a0
47. Singh NK, Wang YX, Wen CN, et al. High-affinity one-step aptamer selection using a non-fouling porous hydrogel. *Nat Biotechnol*. 2024;42(8):1224–1231. doi:10.1038/s41587-023-01973-8

48. Deemter D, Oller I, Amat AM, Malato S. Advances in membrane separation of urban wastewater effluents for (pre) concentration of micro-contaminants and nutrient recovery: a mini review. *Chem Eng J Adv*. 2022;11:100298. doi:10.1016/j.cej.2022.100298
49. Bunka DHJ, Platonova O, Stockley PG. Development of aptamer therapeutics. *Curr Opin Pharmacol*. 2010;10(5):557–562. doi:10.1016/j.coph.2010.06.009
50. Binning JM, Leung DW, Amarasinghe GK. Aptamers in virology: recent advances and challenges. *Front Microbiol*. 2012;3:29–34. doi:10.3389/fmicb.2012.00029
51. Tombelli S, Minunni M, Mascini M. Aptamers-based assays for diagnostics, environmental and food analysis. *Biomol Eng*. 2007;24(2):191–200. doi:10.1016/j.bioeng.2007.03.003
52. Bayat P, Nosrati R, Alibolandi M, et al. SELEX methods on the road to protein targeting with nucleic acid aptamers. *Biochimie*. 2018;154:132–155. doi:10.1016/j.biochi.2018.09.001
53. Wong KY, Liu YB, Wong MS, Liu JW. Cornea-SELEX for aptamers targeting the surface of eyes and liposomal drug delivery. *Exploration-Proc*. 2024;4(4).
54. Wang JF, Chen D, Huang WT, Yang NJ, Yuan Q, Yang YB. Aptamer-functionalized field-effect transistor biosensors for disease diagnosis and environmental monitoring. *Exploration-Proc*. 2023;3(3).
55. Escudero-Abarca BI, Suh SH, Moore MD, Dwivedi HP, Jaykus LA. Selection, characterization and application of nucleic acid aptamers for the capture and detection of human norovirus strains. *PLoS One*. 2014;9(9):e106805. doi:10.1371/journal.pone.0106805
56. Beier R, Pahlke C, Quenzel P, et al. Selection of a DNA aptamer against norovirus capsid protein VP1. *Fems Microbiol Lett*. 2014;351(2):162–169. doi:10.1111/1574-6968.12366
57. Moore MD, Escudero-Abarca BI, Suh SH, Jaykus LA. Generation and characterization of nucleic acid aptamers targeting the capsid P domain of a human norovirus GII.4 strain. *J Biotechnol*. 2015;209:41–49. doi:10.1016/j.jbiotec.2015.06.389
58. Giamberardino A, Labib M, Hassan EM, et al. Ultrasensitive norovirus detection using DNA aptasensor technology. *PLoS One*. 2013;8(11):e79087. doi:10.1371/journal.pone.0079087
59. Schilling KB, DeGrasse J, Woods JW. The influence of food matrices on aptamer selection by SELEX (systematic evolution of ligands by exponential enrichment) targeting the norovirus P-Domain. *Food Chem*. 2018;258:129–136. doi:10.1016/j.foodchem.2018.03.054
60. Liu DL, Zhang ZL, Yin YJ, et al. Development and evaluation of a novel target-capture approach for aptamer selection of human noroviruses. *Talanta*. 2019;193:199–205. doi:10.1016/j.talanta.2018.09.084
61. Qiao WH, Wang SX, Zhang C, Huang Z. A split NanoLuc complementation-based human norovirus-like particle entry assay facilitates evaluation of anti-norovirus antibodies in live cells. *Antiviral Res*. 2022;197:105231. doi:10.1016/j.antiviral.2021.105231
62. Kimura M, Sekiguchi K, Okitsu S, Ushijima H, Tani H. A highly quantitative detection system for cell entry of human norovirus-like particles based on the complementation of NanoLuc luciferase. *Virology*. 2022;573:23–28. doi:10.1016/j.virol.2022.06.001
63. Pfaffl MW. A new mathematical model for relative quantification in real-time RT-PCR. *Nucleic Acids Res*. 2001;29(9):e45. doi:10.1093/nar/29.9.e45
64. Zuker M. Mfold web server for nucleic acid folding and hybridization prediction. *Nucleic Acids Res*. 2003;31(13):3406–3415. doi:10.1093/nar/gkg595
65. Moe CL, Sair A, Lindesmith L, Estes MK, Jaykus LA. Diagnosis of Norwalk virus infection by indirect enzyme immunoassay detection of salivary antibodies to recombinant Norwalk virus antigen. *Clin Diagn Lab Immunol*. 2004;11(6):1028–1034. doi:10.1128/CDLI.11.6.1028-1034.2004
66. Rodríguez-Lázaro D, Hernández M, Scortti M, Esteve T, Vazquez-Boland JA, Pla M. Quantitative detection of *Listeria monocytogenes* and *Listeria innocua* by real-time PCR: assessment of hly, iap, and lin02483 targets and AmpliFluor technology. *Appl Environ Microbiol*. 2004;70(3):1366–1377. doi:10.1128/AEM.70.3.1366-1377.2004
67. Ebel GD, Dupuis AP, Nicholas D, Young D, Maffei J, Kramer LD. Detection by enzyme-linked immunosorbent assay of antibodies to West Nile virus in birds. *Emerg Infect Dis*. 2002;8(9):979–982. doi:10.3201/eid0809.020152
68. Van Beek J, De Graaf M, Al-Hello H, et al. Molecular surveillance of norovirus, 2005–16: an epidemiological analysis of data collected from the NoroNet network. *Lancet Infect Dis*. 2018;18(5):545–553. doi:10.1016/S1473-3099(18)30059-8
69. Kato T, Yano K, Ikebukuro K, Karube I. Interaction of three-way DNA junctions with steroids. *Nucleic Acids Res*. 2000;28(9):1963–1968. doi:10.1093/nar/28.9.1963
70. Ruckman J, Green LS, Beeson J, et al. 2'-Fluoropyrimidine RNA-based aptamers to the 165-amino acid form of vascular endothelial growth factor (VEGF165). Inhibition of receptor binding and VEGF-induced vascular permeability through interactions requiring the exon 7-encoded domain. *J Biol Chem*. 1998;273(32):20556–20567. doi:10.1074/jbc.273.32.20556
71. Bock LC, Griffin LC, Latham JA, Vermaas EH, Toole JJ. Selection of single-stranded-DNA molecules that bind and inhibit human thrombin. *Nature*. 1992;355(6360):564–566. doi:10.1038/355564a0
72. Huizenga DE, Szostak JW. A DNA aptamer That binds adenosine and ATP. *Biochemistry-US*. 1995;34(2):656–665. doi:10.1021/bi00002a033
73. Pollard TD. A guide to simple and informative binding assays. *mol Biol Cell*. 2010;21(23):4061–4067. doi:10.1091/mbc.e10-08-0683
74. Manuel CS, Moore MD, Jaykus LA. Predicting human norovirus infectivity - Recent advances and continued challenges. *Food Microbiol*. 2018;76:337–345. doi:10.1016/j.fm.2018.06.015
75. Hirneisen KA, Kniel KE. Comparison of ELISA attachment and infectivity assays for murine norovirus. *J Virol Methods*. 2012;186(1–2):14–20. doi:10.1016/j.jviromet.2012.07.018
76. Li X, Chen H. Evaluation of the porcine gastric mucin binding assay for high-pressure-inactivation studies using murine norovirus and Tulane virus. *Appl Environ Microbiol*. 2015;81(2):515–521. doi:10.1128/AEM.02971-14
77. Wang DP, Xu SX, Yang D, Young GM, Tian P. New capture quantitative (real-time) reverse transcription-PCR method as an alternative approach for determining inactivation of Tulane virus. *Appl Environ Microbiol*. 2014;80(7):2120–2124. doi:10.1128/AEM.04036-13
78. Moore MD, Bobay BG, Mertens B, Jaykus LA, Coyne CB. Human norovirus aptamer exhibits high degree of target conformation-dependent binding similar to that of receptors and discriminates particle functionality. *mSphere*. 2016;1(6):e00298–00216. doi:10.1128/mSphere.00298-16
79. Faircloth J, Moore MD, Stoufer S, Kim M, Jaykus LA. Generation of nucleic acid aptamer candidates against a novel Calicivirus protein target. *Viruses*. 2021;13(9):1716–1728. doi:10.3390/v13091716
80. Keefe AD, Pai S, Ellington A. Aptamers as therapeutics. *Nat Rev Drug Discov*. 2010;9(7):537–550. doi:10.1038/nrd3141
81. Tan MTH, Li Y, Eshaghi Gorji M, Gong Z, Li D. Fucoidan but not 2'-fucosyllactose inhibits human norovirus replication in zebrafish larvae. *Viruses*. 2021;13(3):461–470. doi:10.3390/v13030461

82. Bentham M, Holmes K, Forrest S, Rowlands DJ, Stonehouse NJ. Formation of higher-order foot-and-mouth disease virus 3D(pol) complexes is dependent on elongation activity. *J Virol.* 2012;86(4):2371–2374. doi:10.1128/JVI.05696-11
83. Moore MD, Cookson J, Coventry VK, Sproat B, Rabe L, Cranston RD. Protection of HIV neutralizing aptamers against rectal and vaginal nucleases: implications for RNA-based therapeutics. *J Biol Chem.* 2011;286(4):2526–2535. doi:10.1074/jbc.M110.178426
84. Wheeler LA, Trifonova R, Vrbanc V, et al. Inhibition of HIV transmission in human cervicovaginal explants and humanized mice using CD4 aptamer-siRNA chimeras. *J Clin Invest.* 2011;121(6):2401–2412. doi:10.1172/JCI45876
85. Hwang SY, Sun HY, Lee KH, et al. 5'-Triphosphate-RNA-independent activation of RIG-I via RNA aptamer with enhanced antiviral activity. *Nucleic Acids Res.* 2012;40(6):2724–2733. doi:10.1093/nar/gkr1098
86. Ayyar BV, Ettayebi K, Salmen W, et al. CLIC and membrane wound repair pathways enable pandemic norovirus entry and infection. *Nat Commun.* 2023;14(1):1148–1161. doi:10.1038/s41467-023-36398-z
87. Liu R, Zhang F, Sang Y, Liu M, Shi M, Wang X. Selection and characterization of DNA aptamers for constructing aptamer-AuNPs colorimetric method for detection of AFM1. *Foods.* 2022;11(12):1802.
88. Wang LL, Lee JY, Gao LF, et al. A DNA aptamer for binding and inhibition of DNA methyltransferase 1. *Nucleic Acids Res.* 2019;47(22):11527–11537. doi:10.1093/nar/gkz1083
89. Yang MH, Li CH, Ye GG, et al. Aptamers targeting SARS-CoV-2 nucleocapsid protein exhibit potential anti pan-coronavirus activity. *Signal Transduct Target Ther.* 2024;9(1). doi:10.1038/s41392-024-01748-w
90. Lesnik EA, Freier SM. Relative thermodynamic stability of DNA, RNA, and DNA-RNA hybrid duplexes - relationship with base composition and structure. *Biochemistry-U.S.* 1995;34(34):10807–10815. doi:10.1021/bi00034a013
91. Sekkal D, Dausse E, Di Primo C, Darfeuille F, Boiziau C, Toulmé JJ. In vitro selection of DNA aptamers against the HIV-1 TAR RNA hairpin. *Antisense Nucleic Acid Drug Dev.* 2002;12(4):265–274. doi:10.1089/108729002320351584
92. Jeon SH, Kayhan B, Ben-Yedidia T, Arnon R. A DNA aptamer prevents influenza infection by blocking the receptor binding region of the viral hemagglutinin. *J Biol Chem.* 2004;279(46):48410–48419. doi:10.1074/jbc.M409059200
93. Khati M, Schüman M, Ibrahim J, Sattentau Q, Gordon S, James W. Neutralization of infectivity of diverse R5 clinical isolates of human immunodeficiency virus type 1 by gp120-binding 2'F-RNA aptamers. *J Virol.* 2003;77(23):12692–12698. doi:10.1128/JVI.77.23.12692-12698.2003

International Journal of Nanomedicine

Publish your work in this journal

The International Journal of Nanomedicine is an international, peer-reviewed journal focusing on the application of nanotechnology in diagnostics, therapeutics, and drug delivery systems throughout the biomedical field. This journal is indexed on PubMed Central, MedLine, CAS, SciSearch®, Current Contents®/Clinical Medicine, Journal Citation Reports/Science Edition, EMBase, Scopus and the Elsevier Bibliographic databases. The manuscript management system is completely online and includes a very quick and fair peer-review system, which is all easy to use. Visit <http://www.dovepress.com/testimonials.php> to read real quotes from published authors.

Submit your manuscript here: <https://www.dovepress.com/international-journal-of-nanomedicine-journal>

Dovepress
Taylor & Francis Group